



Published in final edited form as:

*Proc SPIE Int Soc Opt Eng.* 2017 October ; 10572: . doi:10.1117/12.2286736.

## Cranial thickness changes in early childhood

Niharika Gajawelli<sup>a,b</sup>, Sean Deoni<sup>c,d</sup>, Jie Shi<sup>e</sup>, Holly Dirks<sup>d</sup>, Marius George Linguraru<sup>h,i</sup>,  
Marvin D. Nelson<sup>f,g</sup>, Yalin Wang<sup>e</sup>, and Natasha Lepore<sup>a,b,f</sup>

<sup>a</sup>CIBORG Lab, Department of Radiology, Children's Hospital Los Angeles, CA, USA

<sup>b</sup>Department of Biomedical Engineering, University of Southern California, CA, USA

<sup>c</sup>Department of Pediatric Radiology Research, Children's Hospital Colorado, CO, USA

<sup>d</sup>Department of Biomedical Engineering, Brown University, RI, USA

<sup>e</sup>Department of Computer Science, Arizona State University, AZ, USA

<sup>f</sup>Department of Radiology, University of Southern California, CA, USA

<sup>g</sup>Department of Radiology, Children's Hospital Los Angeles, CA, USA

<sup>h</sup>Sheikh Zayed Institute for Pediatric Surgical Innovation, Children's National Health System, Washington DC

<sup>i</sup>School of Medicine and Health Sciences, George Washington University, Washington DC

### Abstract

The neurocranium changes rapidly in early childhood to accommodate the developing brain. However, developmental disorders may cause abnormal growth of the neurocranium, the most common one being craniosynostosis, affecting about 1 in 2000 children. It is important to understand how the brain and neurocranium develop together to understand the role of the neurocranium in neurodevelopmental outcomes. However, the neurocranium is not as well studied as the human brain in early childhood, due to a lack of imaging data. CT is typically employed to investigate the cranium, but, due to ionizing radiation, may only be used for clinical cases. However, the neurocranium is also visible on magnetic resonance imaging (MRI). Here, we used a large dataset of MRI images from healthy children in the age range of 1 to 2 years old and extracted the neurocranium. A conformal geometry based analysis pipeline is implemented to determine a set of statistical atlases of the neurocranium. A growth model of the neurocranium will help us understand cranial bone and suture development with respect to the brain, which will in turn inform better treatment strategies for neurocranial disorders.

### Keywords

Neurocranium; brain; neonatal/pediatric imaging

## 1. INTRODUCTION

Shape abnormalities of the cranium are associated with some developmental disorders, and early detection in children is important for better treatment and to improve quality of life. The newborn neurocranium consists of tiny bony plates of ossified bone tissue, which are

connected by the soft connective tissue of the sutures and fontanelles. This flexible construction allows the neurocranium to deform or expand to accommodate the rapidly growing brain in early childhood. The cranium expands rapidly from 25% of its adult size at birth to 90% of its adult size by age 4–5<sup>1,2</sup>. The brain, meanwhile, reaches 95% of its final volume by the age of 6.

A normative database of neurocranial development would be of great help for both early detection of abnormalities in the clinic and for surgical planning. For example, craniosynostosis is challenging to diagnose, however, some studies have shown that it may be associated with neurodevelopmental deficits if left undiagnosed or even if treated early<sup>3,4</sup>. Understanding normal variations in cranial shape with age is also important in diagnosing head trauma in children. According to<sup>5</sup>, pediatric cranial sutures deform 30 times more than the cranial bone before failure, and 243 times more than the adult cranial bone. Hence, the cranium may be subjected to major shape changes under trauma, impacting the brain as well. There has also been an increased interest in optimization of surgical procedures for craniosynostosis, especially metopic craniosynostosis, as described in<sup>6,7</sup>. For surgery, it is important to understand the degree of malformation to choose the appropriate surgical intervention. Currently, surgical decisions and normal cranial shape reconstruction vary depending on the subjective assessment of the surgeon<sup>6,7</sup>, so a normative database would be allow a more objective determination of surgical plans.

It is also currently not well understood how the brain and cranial shape parameters co-evolve<sup>8</sup>. For example, studies have shown that environmental factors such as sleep position may also affect neurocranial shape and lead to developmental delays, such as in deformational plagiocephaly<sup>9,10</sup>. Some recent studies have shown that children with deformational plagiocephaly have motor delays in early childhood<sup>10</sup>. It is therefore important to understand neurocranial growth in order detect joint deformities in the cranium and brain at an early stage.

Neurocranium disorders are typically diagnosed via CT images, however, due to ionizing radiation, it is more challenging to build a growth map of shape changes of the neurocranium in healthy children using this modality. In this study, we utilize the fact that the neurocranium can also be delineated on MRI, and take advantage of a large database of MRI scans of healthy children ranging in age from 0–2 years old, acquired at the Baby Imaging Lab [<http://www.babyimaginglab.com>], to map shape changes of the neurocranium in children 1–2 years old.

Among shape parameters, neurocranium thickness in particular is important for understanding the healing process after cranial surgery in diseases such as craniosynostosis and to understand the impacts traumatic brain injury has on the pediatric neurocranium<sup>11,12</sup>. Templates of neurocranium thickness can also be incorporated into epilepsy surgery and can be used for more accurate modeling of the EEG sources<sup>13,14</sup>

To map the change in thickness across various ages, we build tetrahedral meshes for each of the neurocrania. We then apply a discrete Laplace-Beltrami operator<sup>15,16</sup> and solve the

Laplace equation to compute the thickness of the neurocranium. Thickness is then statistically compared between age groups at each vertex of the surface grid.

## 2. METHOD

### Data

The dataset used was of 27 MRI scans (including male and female subjects) of children of ages 12 months, 18 months and 24 months. All data are acquired on a Siemens 3T Tim Trio scanner equipped with a 12 channel head RF array. To minimize intra-scan motion, children are swaddled with a pediatric MedVac vacuum immobilization bag (CFI Medical Solutions, USA) and foam cushions. Scanner noise is reduced by lessening the peak gradient amplitudes and slew-rates, and using a noise-insulating scanner bore insert (Quiet Barrier HD Composite, UltraBarrier, USA).

### Pre-Processing

We used the following pre-processing pipeline for our data analysis. First, the anatomical T1-weighted dataset was skull stripped using FSL BET<sup>17</sup> and resampled to a  $1 \times 1 \times 1 \text{mm}^3$  resolution for consistency throughout the processing. The resampled image was bias corrected using the N4 ANTs bias correction tool<sup>18</sup>. The result was then registered to an age-matched template, which was generated from the same dataset and also resampled to  $1 \times 1 \times 1 \text{mm}^3$  resolution, using FSL FLIRT<sup>19,20</sup> using 6 degrees of freedom. The transformation from FSL FLIRT was saved and applied to the original non-neurocranium stripped dataset. The resulting registered image was then bias corrected using the N4 ANTS bias correction tool again before applying the FSL BET software<sup>17,21</sup>, which includes functionality for getting an outline of the inner and outer neurocranium surfaces. Each mask was visually inspected to ensure accuracy. After visual inspection, we chose the datasets with the clearest delineation of the neurocranium mask for this study specifically. These datasets had the least amount of motion and image artefacts, and the boundaries of the brain, dura and scalp were clearly visible on the image. The dataset consists of 9 datasets for the 12 month cohort, 8 datasets for the 18 month cohort and 10 datasets for the 24 month cohort.

### Thickness Calculation

Using the iso2mesh toolbox<sup>22</sup>, we created volumetric tetrahedral meshes for the inner and outer neurocranium masks, respectively. This toolbox was also used to ensure correct directionality of the normal vectors of the mesh faces generated. The outer neurocranium volumetric mesh generated from the outer neurocranium mask was then separated into the outer and inner surface meshes to calculate the thickness. The thickness calculation involved a similar approach to that used for the corpus callosum in<sup>15,16</sup>. The neurocranial surface was first represented as a boundary of a tetrahedral mesh and then divided into superior and inferior patches. We then computed a harmonic field using a Laplacian operator with Dirichlet boundary conditions. This was done in order to minimize harmonic energy on the mesh and subsequently, streamlines were used to connect the inner and outer surfaces of the neurocranium. Thickness was defined as the total arc length of the streamline from the superior to the inferior patches.

Next, we used the weighted-SPHARM approach described in <sup>23,24</sup> to register the thickness of each individual subject to a common template. This enabled us to get a surface with the same number of vertices, allowing us to compare thickness between groups. Each neurocranium's interior and exterior surfaces were mapped to a sphere using an area preserving surface flattening, described in <sup>25</sup>. A sphere was used to make use of the closeness of the shape of the neurocranium. We used a template sphere with 40962 vertices to compute the spherical harmonic coefficients in order to get a SPHARM representation of the surfaces. Finally, we applied vertex-wise two sample t-tests for thickness comparison between the groups as follows: 12m vs 18m, 18m vs 24m, and 12m vs 24m.

### 3. RESULTS

Results below show the significant p-values (0–0.5) mapped onto a template neurocranium, reconstructed from the SPHARM representation. The blacked out regions in the rest of the neurocranium are not significant and the intensity has been reduced to zero for better visualization. The darker red regions show higher significance closer to 0 and the lighter areas show significance closer to 0.05 as shown in the color bar.

### 4. DISCUSSION

Results above show the regions of the neurocranium that vary the most across comparison of the two groups. If we focus on the areas marked with a red dotted circle, the top image in Fig. 1 shows significant changes in the posterior part of the neurocranium, corresponding to part of the sagittal suture. The pattern shown in the right figure of the top row in the area of the lambdoid suture. This is intuitive as we expect to see greater differences near the sutures that accommodate the growing brain. In addition, according to <sup>26</sup>, the lambdoid suture closes between the age of 1 and 1.5.

The middle figure showing significant differences between the 12m and 24m groups results in a pattern similar to the comparison of the 12m and 18m groups. The least difference was found between the 18m and 24m groups, only showing significant thickness difference in the occipital bone. This indicates that a large portion of the neurocranium thickness change happens prior to 1.5 years. We plan on investigating younger age groups (3 months to 1 year old) in follow up studies to gain a better understanding of early neurocranial growth. The thickness differences found here are consistent with studies done using CT data <sup>26</sup>. For example, the authors in <sup>26</sup> showed a greater thickness of the neurocranium in the occipital region in ages 1.5 years and older.

Cranial growth has also been investigated using non-invasive 3D optical surface scanner data in children of 6–12 months of age <sup>27</sup>, where, it was shown that the head grows more in length (2.84%), by measurement in the head circumference increase. At the same time, the total cranial volume increased by 18.76% <sup>27</sup>. Our study, in addition to using non-invasive MRI, investigates local rather than global changes of the neurocranium, i.e. the thickness.

The neurocranium growth model described here will be improved in our future work by inclusion of more subjects. In this pilot study, we show that using head MRI scans, neurocranial thickness growth can be mapped out to show local changes in thickness. Future

work will include a correlation of the cranial thickness and parameters acquired from the brain, such as cortical thickness, which will allow us to acquire a more complete picture of the co-development of the brain and neurocranium.

## References

1. Bastir M, Rosas A, O'higgins P. Craniofacial levels and the morphological maturation of the human skull. *J Anat.* 209(5):637–654.2006; [PubMed: 17062021]
2. Sperber, GH, Sperber, SM, Guttmann, GD, Sperber, GH. Craniofacial embryogenetics and development. People's Medical Pub. House; USA: 2010.
3. Da Costa AC, Anderson VA, Savarirayan R, Wrennall JA, Chong DK, Holmes AD, Greensmith AL, Meara JG. Neurodevelopmental functioning of infants with untreated single-suture craniosynostosis during early infancy. *Child's Nerv Syst.* 28(6):869–877.2012; [PubMed: 22246335]
4. Chieffo D, Tamburrini G, Massimi L, Di Giovanni S, Giansanti C, Caldarelli M, Di Rocco C. Long-term neuropsychological development in single-suture craniosynostosis treated early. *J Neurosurg Pediatr.* 5(3):232–237.2010; [PubMed: 20192638]
5. Coats B, Margulies SS. Material properties of human infant skull and suture at high rates. *J Neurotrauma.* 23(8):1222–1232.2006; [PubMed: 16928180]
6. Porras AR, Zukic D, Equobahrie A, Rogers GF, Linguraru MG. Personalized Optimal Planning for the Surgical Correction of Metopic Craniosynostosis. *Clin image-based Proced from Plan to Interv Int Work CLIP ...*, held conjunction with MICCAI .. Revis Sel Pap CLIP. 2016:60–67.2016;
7. Mendoza CS, Safdar N, Okada K, Myers E, Rogers GF, Linguraru MG. Personalized assessment of craniosynostosis via statistical shape modeling. *Med Image Anal.* 18(4):635–646.2014; [PubMed: 24713202]
8. Richtsmeier JT, Aldridge K, DeLeon VB, Panchal J, Kane AA, Marsh JL, Yan P, Cole TM. Phenotypic integration of neurocranium and brain. *J Exp Zool B Mol Dev Evol.* 306(4):360–378.2006; [PubMed: 16526048]
9. Robinson S, Proctor M. Diagnosis and management of deformational plagiocephaly. *J Neurosurg Pediatr.* 3(4):284–295.2009; [PubMed: 19338406]
10. Collett BR, Starr JR, Kartin D, Heike CL, Berg J, Cunningham ML, Speltz ML. Development in Toddlers With and Without Deformational Plagiocephaly. *Arch Pediatr Adolesc Med.* 165(7): 653.2011; [PubMed: 21727278]
11. Li Z, Han X, Ge H, Ma C. A semi-automatic method of generating subject-specific pediatric head finite element models for impact dynamic responses to head injury. *J Mech Behav Biomed Mater.* 60:557–567.2016; [PubMed: 27058003]
12. Pinto PS, Poretti A, Meoded A, Tekes A, Huisman TAGM. The Unique Features of Traumatic Brain Injury in Children. Review of the Characteristics of the Pediatric Skull and Brain, Mechanisms of Trauma, Patterns of Injury, Complications and Their Imaging Findings-Part 1. *J Neuroimaging.* 22(2):e1–e17.2012;
13. Cuffin BN. Effects of local variations in skull and scalp thickness on EEG's and MEG's. *IEEE Trans Biomed Eng.* 40(1):42–48.1993; [PubMed: 8468075]
14. Chauveau N, Franceries X, Doyon B, Rigaud B, Morucci JP, Celsis P. Effects of skull thickness, anisotropy, and inhomogeneity on forward EEG/ERP computations using a spherical three-dimensional resistor mesh model. *Hum Brain Mapp.* 21(2):86–97.2004; [PubMed: 14755596]
15. Wang Y, Song Y, Chou Y-Y, Toga AW, Thompson PM. Hippocampal and Ventricular Differences in 804 ADNI subjects mapped with Multivariate Tensor-Based Morphometry.
16. Xu L, Collignon O, Wang G, Kang Y, Leporé F, Shi J, Lao Y, Joshi A, Leporé N, Wang Y. Combining Thickness Information with Surface Tensor-based Morphometry for the 3D Statistical Analysis of the Corpus Callosum. 2013
17. Smith SM. Fast robust automated brain extraction. *Hum Brain Mapp.* 17(3):143–155.2002; [PubMed: 12391568]
18. Tustison NJ, Avants BB, Cook PA, Egan A, Yushkevich PA, Gee JC. N4ITK: Improved N3 Bias Correction. *IEEE Trans Med Imaging.* 29(6):1310–1320.2010; [PubMed: 20378467]

19. Jenkinson M, Smith S. A global optimisation method for robust affine registration of brain images. *Med Image Anal.* 5(2):143–156.2001; [PubMed: 11516708]
20. Jenkinson M, Bannister P, Brady M, Smith S. Improved optimization for the robust and accurate linear registration and motion correction of brain images. *Neuroimage.* 17(2):825–841.2002; [PubMed: 12377157]
21. Jenkinson M; Pechaud, M; Smith, S. BET2: MR-based estimation of brain, skull and scalp surfaces. Eleventh Annual Meeting of the Organization for Human Brain Mapping; 2005.
22. Boas, DA. 2009 IEEE Int Symp Biomed Imaging From Nano to Macro. IEEE; 2009. Tetrahedral mesh generation from volumetric binary and grayscale images; 1142–1145.
23. Chung MK, Dalton KM, Davidson RJ. Tensor-based cortical surface morphometry via weighted spherical harmonic representation. *IEEE Trans Med Imaging.* 27(8):1143–1151.2008; [PubMed: 18672431]
24. Chung, MK. *Computational Neuroanatomy: The Methods.* World Scientific; 2012.
25. Chung, MK. MIDUS Amygdala/Hippocampus Surface Data Set, SPHARM and the Random Field Theory Based Surface Data Analysis Pipeline. <<http://brainimaging.waisman.wisc.edu/~chung/midus/>>
26. Li, Z, Park, B-K, Liu, W, Zhang, J, Reed, MP, Rupp, JD, Hoff, CN, Hu, J. A Statistical Skull Geometry Model for Children 0–3 Years Old. In: Cray, J, Jr, editor. *PLoS One.* Vol. 10. 2015. e0127322
27. Meyer-Marcotty P, Böhm H, Linz C, Kochel J, Stellzig-Eisenhauer A, Schweitzer T. Three-dimensional analysis of cranial growth from 6 to 12 months of age. *Eur J Orthod.* 36(5):489–496.2014; [PubMed: 25257925]

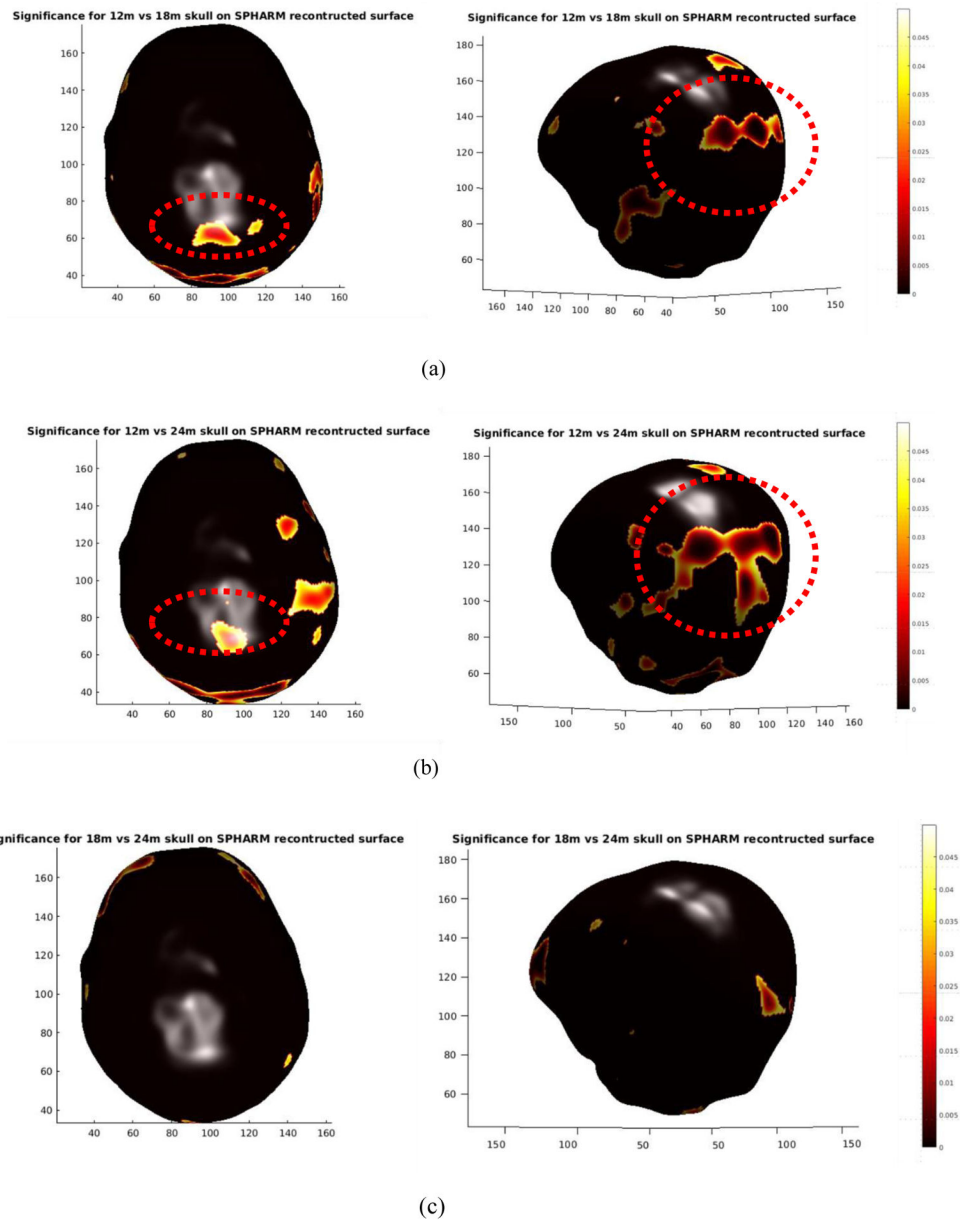


**Figure 1.**

(a) Significant p-values that result in the comparison of the 12m and 18m groups. (b) Significant p-values that result in the comparison of the 12m and 24m groups. (c) Significant p-values that result in the comparison of the 18m and 24m groups. The red circles indicate areas that are consistent patterns when compared with other studies.